Spin and orbital magnetic moments in perpendicularly magnetized $Ni_{1-x}Co_{2+y}O_{4-z}$ epitaxial thin films: Effects of site-dependent cation valence states

Daisuke Kan,[1,*] Masaichiro Mizumaki,[2] Miho Kitamura,[3] Yoshinori Kotani,[2] Yufan Shen,[1] Ikumi Suzuki,[1] Koji Horiba,[3] and Yuichi Shimakawa[1]

[1]*Institute for Chemical Research, Kyoto University, Uji, Kyoto 611-0011, Japan*

[2]*Japan Synchrotron Radiation Research Institute, SPring-8, Sayo, Hyogo 679-5198, Japan*

[3]*Photon Factory, Institute of Materials Structure Science, High Energy Accelerator Research Organization (KEK), Tsukuba 305-0801, Japan*

(Received 19 February 2020; revised manuscript received 20 April 2020; accepted 9 June 2020; published 26 June 2020)

We carried out x-ray absorption spectroscopy (XAS) and x-ray magnetic circular dichroism (XMCD) spectroscopy and investigated cation valence states and spin and orbital magnetic moments in inverse-spinel ferrimagnet $Ni_{1-x}Co_{2+y}O_{4-z}$ (NCO) epitaxial films with perpendicular magnetic anisotropy. We show that the oxygen pressure P_{O2} during film growth by pulsed laser deposition influences not only the cation stoichiometry (site occupation) but also the cation valence state. Our XAS results show that the Ni in the O_h-site is in the intermediate valence state between +2 and +3, $Ni^{(2+\delta)+}$ ($0 < \delta < 1$), whose nominal valence state (the δ value) varies depending on P_{O2}. On the other hand, the Co in the octahedral (O_h) and tetrahedral (T_d) sites, respectively, have a valence state close to +3 and +2. We also find that the XMCD signals originate mainly from the T_d-site Co^{2+} (Co_{Td}) and O_h-site $Ni^{(2+\delta)+}$ (Ni_{Oh}), indicating that these cation valence states are the key to determining the magnetic and transport properties of NCO films. Interestingly, the valence state of $Ni^{(2+\delta)+}$ that gives rise to the XMCD signal remains unchanged independent of P_{O2}. The electronic structure of $Ni^{(2+\delta)+}$ that is responsible for the magnetic moment and electrical conduction differs from those of Ni^{2+} and Ni^{3+}. In addition, the orbital magnetic moment originating from Co_{Td} is as large as 0.14 μ_B/Co_{Td} and parallel to the magnetization, while the Ni_{Oh} orbital moment is as small as 0.07 μ_B/Ni_{Oh} and is rather isotropic. Co_{Td}, therefore, plays the key role in the perpendicular magnetic anisotropy of the films. Our results demonstrate the significance of the site-dependent cation valence states for the magnetic and transport properties of $NiCo_2O_4$ films.

DOI: 10.1103/PhysRevB.101.224434

I. INTRODUCTION

Transition metals in oxides can have various valence states through orbital hybridization with oxygen, impacting various functional properties. For ternary spinel oxides, transition metals occupying tetrahedral and octahedral sites can have different valence states, leading to a variety of transport and magnetic properties. It is important, therefore, to evaluate cation valence states in spinel oxides, and to delineate their influence on physical properties.

The inverse spinel oxide $NiCo_2O_4$ [1–5], in which Co is in both tetrahedral (T_d) and octahedral (O_h) sites while Ni is in only the O_h site, has been shown to have a variety of properties, such as above-room-temperature ferrimagnetism [3,5], metallic electrical conduction [6–8], half-metallic properties [6,7], perpendicular magnetic anisotropy [9,10], and electrochemical activities [11–14]. These findings have revealed the potential application of this oxide for spintronic and electrochemical devices. Therefore, delineating correlations between cation valence states and functional properties in $NiCo_2O_4$ is crucial. Recently, it has been shown that the transport and magnetic properties of epitaxial films of this oxide depend strongly on their growth conditions [6,15–18]. Our resonant x-ray diffraction measurements [19] for films grown by pulsed laser deposition have also revealed that cation distribution (T_d- and O_h-site occupation of Co and Ni) in $NiCo_2O_4$ films varies depending on oxygen partial pressure (P_{O2}'s) during film growth. Given that Co and Ni could accommodate various valence states (+2 and +3, for example), growth conditions such as P_{O2} would influence not only compositions but also valence states of Co and Ni, affecting the films' properties. Thus, it is interesting to see correlations between cation valence states and the physical properties of $NiCo_2O_4$ films grown under various P_{O2}'s.

In this study, we carried out x-ray absorption spectroscopy (XAS) and x-ray magnetic circular dichroism (XMCD) spectroscopy and investigated valence states and spin and orbital magnetic moments of Co and Ni in $Ni_{1-x}Co_{2+y}O_{4-z}$ (NCO) epitaxial films grown under a P_{O2} of 30, 50, and 100 mTorr by pulsed laser deposition. We found that not only the Co- and Ni-site occupations (the Co and Ni compositions) but also their valence states in the films vary depending on P_{O2}. The NCO depositions under lower P_{O2} introduce larger amounts of Co^{2+} and Ni^{2+} into films, influencing their transport and magnetic properties. Furthermore, analyzing XAS and XMCD data quantitatively by the sum rules [20–22], we discuss the origin of the perpendicular magnetic anisotropy in NCO films.

*dkan@scl.kyoto-u.ac.jp

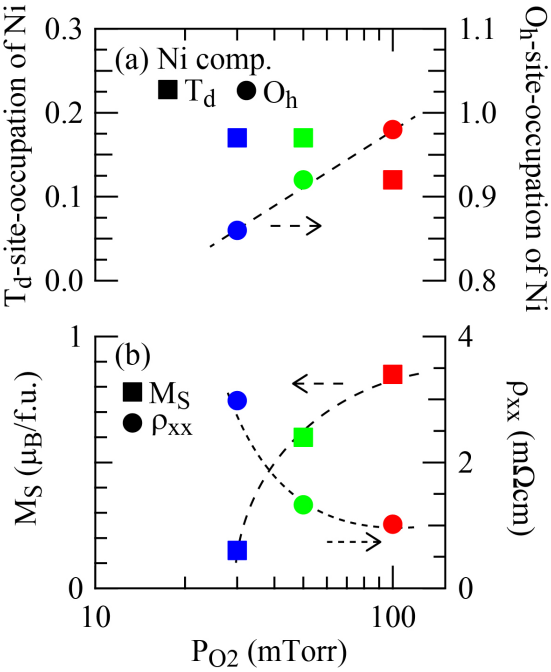

FIG. 1. P_{O2} dependence of (a) the tetrahedral (T_d) and octahedral (O_h) site-occupation of Ni, and (b) saturated magnetization and electrical resistivity in NCO epitaxial films. All data in the figures were taken at room temperature. The data in (a) were adopted from Ref. [19]. We note that the cation site-occupation (cation composition) in the NCO film is defined as $(Co_{y-Co-Td}Ni_{x-Ni-Td})(Co_{y-Co-Oh}Ni_{x-Ni-Oh})O_4$. The T_d- and O_h-site occupations of cations were determined by assuming that $y_{Co-Td} + x_{Ni-Td} = 1$ and $y_{Co-Oh} + x_{Ni-Oh} = 2$.

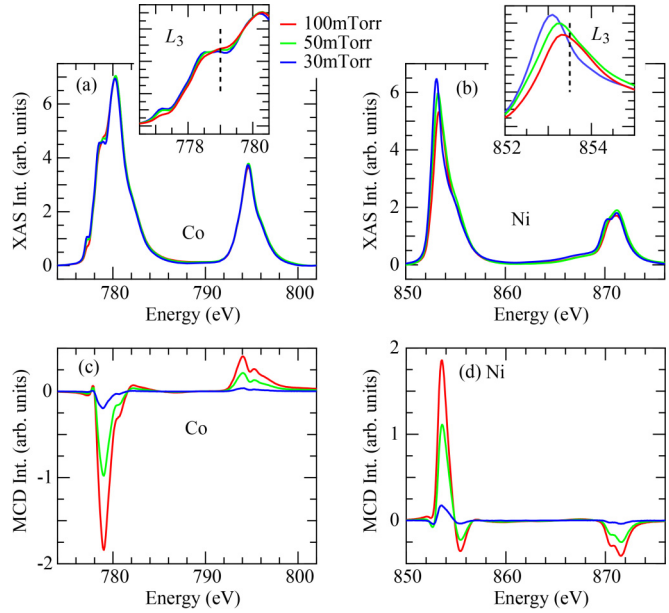

FIG. 2. (a), (b) Averaged XAS and (c), (d) normalized XMCD spectra for NCO films grown under $P_{O2} = 30$, 50, and 100 mTorr. The spectra were in the energy region around (a,c) Co and (b,d) Ni $L_{2,3}$-edge absorptions. The measurements were carried out at room temperature and under a 1.9 T magnetic field normal to the films' surface (the $\theta_H = 0°$ configuration). The incident beam is 10° off the magnetic-field direction θ_H. The insets in parts (a) and (b) show expanded views of the Co and Ni L_3-edge absorption peaks.

II. EXPERIMENTAL DETAILS

30-nm-thick $Ni_{1-x}Co_{2+y}O_{4-z}$ (NCO) epitaxial films with (001) orientation were fabricated on (100) $MgAl_2O_4$ substrates and under various oxygen pressures (P_{O2}'s) by pulsed laser deposition. All films studied here are under substrate-induced compressive strain (0.4%). Previously, we showed [19] that when films were grown at a fixed substrate temperature (350 °C), the P_{O2} affected the cation distribution (or the cation composition) in the films, influencing transport and magnetic properties. Details of the results of basic characterization for grown NCO films, such as x-ray diffraction and magnetization measurements, were provided in our previous report [19]. Briefly, by analyzing x-ray diffraction intensities near the cations' absorption edges, the T_d- and O_h-site occupation of Ni (the amounts of Ni occupying the tetrahedral and octahedral sites) was determined to be 0.17 and 0.86 for the $P_{O2} = 30$ mTorr film, 0.17 and 0.92 for the $P_{O2} = 50$ mTorr film, and 0.12 and 0.98 for the $P_{O2} = 100$ mTorr film. As shown in Fig. 1(a), the T_d-site occupation of Ni is almost constant and independent of P_{O2}. On the other hand, the O_h-site occupation of Ni increases with increasing P_{O2}. In addition, the films grown under larger P_{O2} have larger saturated magnetizations and lower electrical resistivity [Fig. 1(b)]. The ferrimagnetic transition temperature of the films grown under larger P_{O2} also becomes higher, and the $P_{O2} = 100$ mTorr film becomes a ferrimagnet below 400 K [19].

We carried out XAS and XMCD spectroscopy and characterized the NCO films grown under $P_{O2} = 30$, 50, and 100 mTorr. Measurements were carried out at the beamlines BL25SU in SPring-8 [23,24] and BL-16A in Photon Factory. XAS and XMCD datasets presented in this paper are those obtained from measurements in SPring-8. We note that the datasets acquired from measurements at the two beamlines were essentially the same. The XAS and MCD spectra were recorded at room temperature and under a 1.9 T magnetic field applied at various angles θ_H with respect to the films' surface. The incident x-ray beam is 10° off the magnetic-field direction. The energy resolution in XAS and XMCD spectra is $E/\Delta E = 3000$. The XAS spectra for each helicity of the incident beam (μ^+ and μ^-) were obtained in the total electron yield mode and by averaging spectra taken under magnetic fields in opposite directions.

III. RESULTS AND DISCUSSION

Figures 2(a) and 2(b) show the averaged Co and Ni $L_{2,3}$-edge XAS spectra $1/2(\mu^+ + \mu^-)$ for NCO films grown under $P_{O2} = 30$, 50, and 100 mTorr, revealing P_{O2}-dependent changes in the valence states of Co and Ni in the films. The data were taken under a 1.9 T magnetic field normal to the films' surface (the $\theta_H = 0°$ configuration). The incident beam is 10° off the magnetic-field direction θ_H. In Co L_3-edge XAS spectra [Fig. 2(a)], the pre-edge structure around 777.2 eV is pronounced with higher intensity, and the hump structure around 778.8 eV is slightly broader for films grown under lower P_{O2}. On the other hand, the peak intensities

at 780.2 eV are almost constant and independent of P_{O2}. Based on reference spectra of Co oxides such as CoO and $EuCoO_3$ [18,25,26], the pre-edge structure (around 777.2 eV) is characteristic for Co^{2+} octahedrally coordinated by oxygen. The hump (around 778.8 eV) arises from both octahedrally and tetrahedrally coordinated Co^{2+}. On the other hand, the peak at 780.2 eV originates from the Co^{3+} in either tetrahedral or octahedral oxygen coordination. Therefore, the observed P_{O2}-dependent changes in Co L_3-edge XAS spectra indicate that for the film grown under $P_{O2} = 100$ mTorr and having the cation site occupation closer to stoichiometric, the T_d- and O_h-site Co (referred to as Co_{Td} and Co_{Oh}, respectively) dominantly have +2 and +3 valence states, respectively. We also point out that as revealed by our resonant x-ray diffraction measurements [Fig. 1(a)], the film grown under the lower P_{O2} has the larger site occupation of Co_{Oh} while the Co_{Td}-site occupation remains almost unchanged against P_{O2}. The additionally introduced Co_{Oh}, which substitutes the O_h-site Ni, in films grown under lower P_{O2} have +2 valence states. We note that the spectral shape around the Co L_2-edge absorption is known to be less dependent on the valence state (+2 or +3). Therefore, the Co L_2-edge XAS peak at 794.6 eV exhibits no obvious P_{O2} dependence.

The Ni $L_{2,3}$-edge absorption spectra in Fig. 2(b) also depend on P_{O2}. The peak positions of the Ni L_3-edge absorptions for films grown under higher P_{O2} shift toward the higher-energy side. Concomitantly, the shoulder structures associated with the Ni L_2-edge absorptions (around 870.3 eV) are less pronounced for the larger-P_{O2} films. These observations indicate that the Ni in the O_h site is in the intermediate valence state between +2 and +3, $Ni^{(2+\delta)+}$ ($0 < \delta < 1$). We note that the L_3-edge peak position for the $P_{O2} = 30$ mTorr film (853.1 eV) is almost identical to the L_3-edge peak position characteristic of the Ni^{2+} octahedrally coordinated by oxygen (~853 eV) [18,27,28]. In addition, the O_h-site occupation of Ni in the film decreases with decreasing P_{O2} [19]. The P_{O2}-dependent shifts of the Ni L_3-edge absorption peaks, therefore, indicate that growing films under lower P_{O2} leads not only to the decrease in the O_h-site occupation of Ni but also to the lowering of its valence state. The Ni valence state for the $P_{O2} = 30$ mTorr film is closer to +2. By reproducing the experimentally observed Ni XAS spectra based on reference spectra of Ni^{2+} and Ni^{3+} L-edge absorptions [29], the Ni nominal valence state for the $P_{O2} = 100$ mTorr film is estimated to be about +2.5 ($\delta \sim 0.5$) [30]. The observed changes in the valence states of Co and Ni imply that the oxygen content in NCO films also varies depending on P_{O2} and that larger amounts of oxygen vacancies are accommodated in films grown under lower P_{O2} [30].

The P_{O2}-dependent changes in the Co and Ni valence states impact the magnetic properties as revealed by XMCD spectroscopy. Figures 2(c) and 2(d), respectively, show the Co and Ni $L_{2,3}$-edge XMCD spectra for the $P_{O2} = 30$, 50, and 100mTorr films. The XMCD signals ($\Delta\mu = \mu^+ - \mu^-$) are observed in both Co and Ni absorption edges for all the films. While the signal intensities depend on P_{O2}, the whole spectral shapes and the peak positions remain almost unchanged independent of P_{O2}. Both Co and Ni XMCD peaks for the films grown under larger P_{O2} have higher intensities, indicating that both spin magnetic moments of Co and Ni are larger for films having larger magnetization.

Interestingly, the Co L_3-edge XMCD signals are enhanced at 779 eV where the x-ray absorptions of the T_d- and O_h-site Co^{2+} occur, and their magnitudes become larger for the films grown under the larger P_{O2} whose O_h-site occupation of Co^{2+} is smaller. In addition, the O_h-site Co^{3+} should be in the low-spin state with $S = 0$ [1,4,18], and no contribution of Co_{Oh} to the XMCD signal is expected. Therefore, the observed P_{O2} dependence of the Co XMCD signal implies that the spin magnetic moments in the T_d-site Co^{2+} ($S = 3/2$) dominantly contribute to the signal. The Ni L_3-edge XMCD signal in Fig. 2(d) also becomes larger for the films grown under the larger P_{O2} and having the O_h-site Ni with the higher intermediate valence state. While the observed spectral shape of the Ni XMCD signals resembles that characteristic of octahedrally coordinated Ni^{2+} [31], it is unlikely that the Ni^{2+} in the O_h-site, which has the $S = 1$ configuration, gives rise to the XMCD signal. The O_h-site occupations of Ni^{2+} are larger for the films grown under the lower P_{O2} while their Ni XMCD signals are largely suppressed [Fig. 2(d)]. We also note that the energy positions of Ni XMCD signals are constant independent of P_{O2}, which is in contrast to the P_{O2}-dependent variations of the nominal valence of Ni [Fig. 2(b)]. These observations indicate that the Ni with an intermediate valence state, $Ni^{(2+\delta)+}$, is the key for the spin magnetic moment. The electronic structure of $Ni^{(2+\delta)+}$ that gives rise to the XMCD signal differs from those of Ni^{2+} and N^{3+} (and their mixtures).

Our XAS and XMCD results highlight the significance of the T_d-site Co (Co_{Td}) and O_h-site Ni (Ni_{Oh}) as the keys that determine the magnetic and transport properties of NCO films. Recent first-principles calculations showed that the density of states at the Fermi level in stoichiometric NCO consists of spin-down electrons of the Ni_{Oh}, leading to the half-metallic electronic structure [6,7]. Importantly, when the O_h-site Ni has an intermediate valence state (higher than +2), its e_g orbitals are partially unoccupied, and conduction carriers are provided. Given the half-metallic electronic structure in NCO, the delocalization of the conduction carriers should preferably align the spin magnetic moments in each O_h and T_d sublattice. It is worth pointing out that reducing the Ni-site occupation and lowering its valence state results in localization of the conduction carriers, and thus the spin magnetic moments in the films with lowered electrical conduction are more difficult to align. Therefore, the films grown under larger P_{O2} have lower electrical resistivity and larger magnetization (Fig. 1).

We also note that the signs of the Co and Ni XMCD signals are opposite each other, which is further confirmed from the magnetic-field dependences of Co and Ni L_3-edge XMCD signals in Fig. 3. For all films, the Co and Ni signals in the positive magnetic field regions are negative and positive, respectively, indicating that the spin magnetic moments of Co_{Td} and Ni_{Oh} align in an antiparallel manner. The hysteresis behavior of the signals against the magnetic-field sweep direction becomes prominent for the films grown under larger P_{O2}, and the remnant values of both Co and Ni signals at zero magnetic field also become larger. These observations are in close agreement with the fact that the films grown under larger

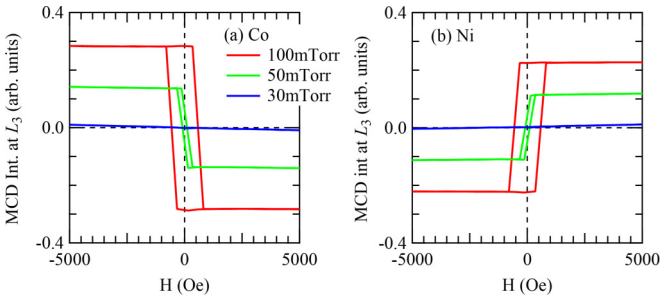

FIG. 3. Magnetic-field dependence of (a) Co L_3- and (b) Ni L_3-XMCD peak intensity for NCO films grown under $P_{O2} = 30$, 50, and 100 mTorr. The data were collected in the $\theta_H = 0°$ configuration and with the incident x-ray energy fixed to be 779.0 eV for the Co L_3 − XMCD signal and 853.5 eV for the Ni signal.

P_{O2} have larger magnetization and a higher ferrimagnetic transition temperature [19].

We further evaluate spin and orbital magnetic moments originating from Ni_{Oh} and Co_{Td} quantitatively, and we investigate how these cations contribute to the orbital magnetic moments that determine the perpendicular magnetic anisotropy in the films. Figure 4 shows the Co and Ni $L_{2,3}$-edge XMCD spectra and their integrated ones obtained with the $\theta_H = 0°$, 40°, and 80° configurations. The inset of the figure schematically shows the measurement configuration including the magnetic-field angle θ_H. The Co L_3-edge XMCD peak intensities and the integrated XMCD signals decrease with increasing θ_H. In contrast, while the Ni XMCD signals and their integrated intensities vary slightly against the change in θ_H, no clear relationships between the signal variations and θ_H are seen. Given that the value obtained by integrating the L_2 and L_3 XMCD peaks is proportional to the orbital magnetic moment according to the sum rules [20–22], the θ_H dependence observed in the Co and Ni XMCD signals implies that the orbital magnetic moment of Co is anisotropic whereas that of Ni is rather symmetric, indicating that the Co plays

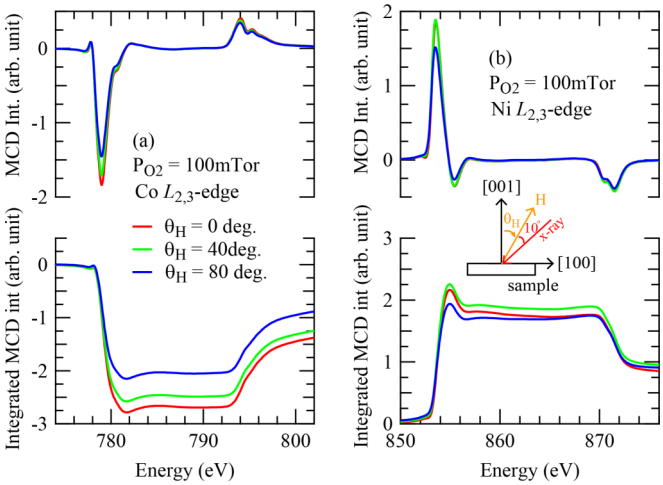

FIG. 4. (a) Co $L_{2,3}$- and (b) Ni $L_{2,3}$-XMCD spectra and their integrated intensity for the $P_{O2} = 100$ mTorr film. The spectra were measured with the magnetic-field angle θ_H of 0°, 40°, and 80°. The measurement configuration is shown in the inset of the figure.

the dominant role in determining the magnetic anisotropy in NCO.

To quantitatively evaluate orbital and spin magnetic moments, we applied the sum rules to the XAS and XMCD spectra obtained at various θ_H and calculated the moments. We note that the Co XMCD signals mainly originate from the Co_{Td} dominantly having the +2 valence state while none of the Co_{Oh} contribute to the magnetic moment. The number of electrons in 3*d* orbitals, n_{3d}, for Co is thus assumed to be 7 (corresponding to Co^{2+}). Taking into account that the energy position of the Ni L_3-edge XMCD peak is close to that of the Ni L_3-edge absorption peak for the $P_{O2} = 100$ mTorr film, as shown in the inset of Fig. 2(b), we assume that the Ni valence state that dominantly contributes to the XMCD signal is +2.5 and the n_{3d} for Ni is 7.5. Figure 5 shows the θ_H dependence of the spin and orbital magnetic moments of Co_{Td} and Ni_{Oh} in the NCO films grown under $P_{O2} = 30$, 50, and 100 mTorr. As expected from the P_{O2} dependence of the XMCD signals (Figs. 2 and 3), the spin magnetic moments of both Co_{Td} and Ni_{Oh} in the films grown under the larger P_{O2} become larger. Both Co_{Td} and Ni_{Oh} spin magnetic moments are θ_H-dependent with their maxima at $\theta_H = 0°$. In addition, the orbital magnetic moments of Co_{Td} and Ni_{Oh} are P_{O2}-dependent, and their trends follow those of the P_{O2} dependence of the spin magnetic moments. For both Co_{Td} and Ni_{Oh}, the orbital and spin moments have the same sign. Thus, the orbital and spin moments are parallel aligned in each T_d and O_h sublattice. Importantly, the Co_{Td} orbital magnetic moment is θ_H-dependent and is maximized at $\theta_H = 0°$ while the Ni_{Oh} orbital magnetic moment is almost θ_H-independent. For the $P_{O2} = 100$ mTorr film whose perpendicular magnetic anisotropy energy is largest among the films investigated in this study [19], the Co_{Td} orbital moment is as large as 0.14 μ_B/Co_{Td} while the Ni_{Oh} one is as small as 0.07 μ_B, indicating that Co_{Td} plays the dominant role in determining the perpendicular anisotropy, and that the contribution of Ni_{Oh} to the magnetic anisotropy is less dominant. This observation is in agreement with the recent theoretical investigation [10] showing that the out-of-plane orbital magnetic moment originates from the d_{x2-y2} orbital in the T_d-site Co, leading to the perpendicular magnetic anisotropy in NCO. Our results indicate the significance of the site-dependent cation valence states for the magnetic and transport properties of $NiCo_2O_4$ films. The Co_{Td} determines the magnetic anisotropy while it provides almost no density of states at the Fermi level and has less influence on the magnetization and electrical conduction of the NCO films. On the other hand, the Ni_{Oh} contributes little to the magnetic anisotropy while it is closely tied to the electronic structure around E_F, strongly influencing the magnetization and the electrical conduction. These correlations between the site-dependent cation states and the functional properties explain why $NiCo_2O_4$ has half-metallic band structure and perpendicular magnetic anisotropy simultaneously.

IV. SUMMARY

We evaluated the cation valence states and spin and orbital magnetic moments in ferrimagnetic $Ni_{1-x}Co_{2+y}O_{4-z}$ (NCO) epitaxial films with perpendicular magnetic anisotropy. We found that the oxygen pressure P_{O2} during film growth by

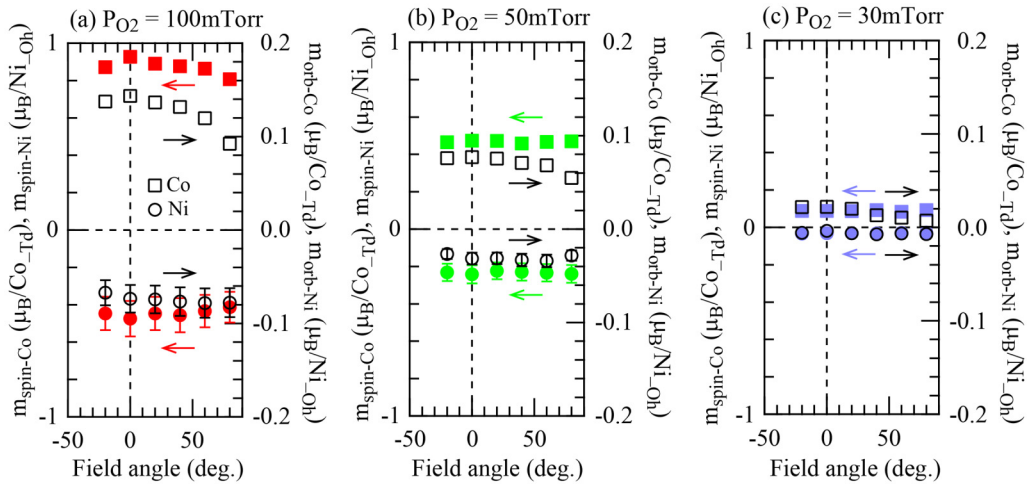

FIG. 5. Magnetic-field angle dependence of spin and orbital magnetic moments (m_{spin} and m_{orb}) originating from the T_d-site Co (Co_{Td}) and the O_h-site Ni (Ni_{Oh}) in NCO films grown under P_{O2} = (a) 100, (b) 50, and (c) 30 mTorr. The filled squares and circles are for the m_{spin} from the Co_{Td} and Ni_{Oh}, respectively. The open squares and circles are for the m_{orb} from the Co_{Td} and Ni_{Oh}, respectively. Errors in the spin and orbital magnetic moments of Ni_{Oh} are estimated from the possible variation of n_{3d}, i.e., $7 < n_{3d} < 8$. In (c), the errors in the Ni moments are not included in the figure because they are relatively small (smaller than the marker sizes).

pulsed laser deposition influences not only the cation stoichiometry but also the cation valence states. For a film having a cation site occupation close to the stoichiometric one, the O_h-site Ni is in the intermediate valence state while the T_d-site and O_h-site Co dominantly have +2 and +3 valence states, respectively. On the other hand, for films grown under the lower P_{O2}, the O_h-site occupation of Ni is reduced, and its valence state is also lowered closer to +2. The Co additionally accommodated in the O_h-site is in the +2 valence state, while the valence state of the T_d-site Co remains unchanged. The spin magnetic moments in the NCO films dominantly originate from the T_d-site Co (Co_{Td}) and the O_h-site Ni (Ni_{Oh}). Both Co_{Td} and Ni_{Oh} spin moments become larger when the cation site occupation is closer to the stoichiometric one. These observations indicate that the intermediate valence state of the Ni_{Oh} is responsible for the delocalization of conduction carriers and plays a key role in stabilizing the electrical conduction and the ferrimagnetic moment. We also show that the orbital magnetic moment originating from Co_{Td} is as large as 0.14 μ_B/Co_{Td} and is anisotropic, parallel to the out-of-plane direction. On the other hand, the Ni_{Oh} orbital moment is as small as $\sim$ 0.07 μ_B/Ni_{Oh} and is rather isotropic. Co_{Td}, therefore, plays the key role in the perpendicular magnetic anisotropy in the films. Our results demonstrate the significance of the site-dependent cation valence states for the magnetic and transport properties of $NiCo_2O_4$ films.

ACKNOWLEDGMENTS

This work was partially supported by a grant for the Integrated Research Consortium on Chemical Sciences, by Grants-in-Aid for Scientific Research (Grants No. JP16H02266, No. JP17H04813, No. JP18K141130, and No. JP19H05816), by a JSPS Core-to-Core program (A), and by a grant for the International Collaborative Research Program of Institute for Chemical Research in Kyoto University from the Ministry of Education, Culture, Sports, Science and Technology (MEXT) of Japan. The synchrotron radiation experiments at Photon Factory were performed with the approval of the Photon Factory Program Advisory Committee (Proposal No. 2019PF-29). The XAS and XMCD measurements at SPring-8 were made with the approval of the Japan Synchrotron Radiation Research Institute (Proposal No. 2019B1266).

[1] J. F. Marco, J. R. Gancedo, M. Gracia, J. L. Gautier, E. Ríos, and F. J. Berry, J. Solid State Chem. **153**, 74 (2000).
[2] D. Pyke, K. K. Mallick, R. Reynolds, and A. K. Bhattacharya, J. Mater. Chem. **8**, 1095 (1998).
[3] O. Knop, K. I. G. Reid, Sutarno, and Y. Nakagawa, Can. J. Chem. **46**, 3463 (1968).
[4] P. D. Battle, A. K. Cheetham, and J. B. Goodenough, Mater. Res. Bull. **14**, 1013 (1979).
[5] J. F. Marco, J. R. Gancedo, M. Gracia, J. L. Gautier, E. I. Ríos, H. M. Palmer, C. Greaves, and F. J. Berry, J. Mater. Chem. **11**, 3087 (2001).
[6] P. F. Ndione, Y. Shi, V. Stevanovic, S. Lany, A. Zakutayev, P. A. Parilla, J. D. Perkins, J. J. Berry, D. S. Ginley, and M. F. Toney, Adv. Funct. Mater. **24**, 610 (2014).
[7] K. Zhang, C. Zhen, W. Wei, W. Guo, G. Tang, L. Ma, D. Hou, and X. Wu, RSC Adv. **7**, 36026 (2017).
[8] M. Wang, X. Sui, Y. Wang, Y.-H. Juan, Y. Lyu, H. Peng, T. Huang, S. Shen, C. Guo, J. Zhang, Z. Li, H.-B. Li, N. Lu, A. T. N'Diaye, E. Arenholz, S. Zhou, Q. He, Y.-H. Chu, W. Duan, and P. Yu, Adv. Mater. **31**, 1900458 (2019).
[9] X. Chen, X. Zhang, M.-G. Han, L. Zhang, Y. Zhu, X. Xu, and X. Hong, Adv. Mater. **31**, 1805260 (2019).

[10] C. Mellinger, J. Waybright, X. Zhang, C. Schmidt, and X. Xu, Phys. Rev. B **101**, 014413 (2020).
[11] J. Zhu and Q. Gao, Microporous Mesoporous Mater. **124**, 144 (2009).
[12] D. P. Dubal, P. Gomez-Romero, B. R. Sankapal, and R. Holze, Nano Energy **11**, 377 (2015).
[13] R. Ding, L. Qi, M. Jia, and H. Wang, Nanoscale **6**, 1369 (2014).
[14] M. U. Anu Prathap and R. Srivastava, Nano Energy **2**, 1046 (2013).
[15] C. Zhen, X. Zhang, W. Wei, W. Guo, A. Pant, X. Xu, J. Shen, L. Ma, and D. Hou, J. Phys. D **51**, 145308 (2018).
[16] P. Silwal, L. Miao, J. Hu, L. Spinu, D. H. Kim, and D. Talbayev, J. Appl. Phys. **114**, 103704 (2013).
[17] P. Silwal, L. Miao, I. Stern, X. Zhou, J. Hu, and D. H. Kim, Appl. Phys. Lett. **100**, 032102 (2012).
[18] Y. Bitla, Y.-Y. Chin, J.-C. Lin, C. N. Van, R. Liu, Y. Zhu, H.-J. Liu, Q. Zhan, H.-J. Lin, C.-T. Chen, Y.-H. Chu, and Q. He, Sci. Rep. **5**, 15201 (2015).
[19] Y. Shen, D. Kan, Z. Tan, Y. Wakabayashi, and Y. Shimakawa, Phys. Rev. B **101**, 094412 (2020).
[20] B. T. Thole, P. Carra, F. Sette, and G. van der Laan, Phys. Rev. Lett. **68**, 1943 (1992).
[21] P. Carra, B. T. Thole, M. Altarelli, and X. Wang, Phys. Rev. Lett. **70**, 694 (1993).
[22] C. T. Chen, Y. U. Idzerda, H. J. Lin, N. V. Smith, G. Meigs, E. Chaban, G. H. Ho, E. Pellegrin, and F. Sette, Phys. Rev. Lett. **75**, 152 (1995).
[23] Y. Senba, H. Ohashi, Y. Kotani, T. Nakamura, T. Muro, T. Ohkochi, N. Tsuji, H. Kishimoto, T. Miura, M. Tanaka, M. Higashiyama, S. Takahashi, Y. Ishizawa, T. Matsushita, Y. Furukawa, T. Ohata, N. Nariyama, K. Takeshita, T. Kinoshita, A. Fujiwara, M. Takata, and S. Goto, in *Proceedings of the 12th International Conference on Synchrotron Radiation Instrumentation - SRI2015*, edited by Q. Shen and C. Nelson,AIP Conf. Proc. No. 1741 (AIP, New York, 2016), p. 030044.
[24] T. Nakamura, T. Muro, F. Z. Guo, T. Matsushita, T. Wakita, T. Hirono, Y. Takeuchi, and K. Kobayashi, J. Electron. Spectrosc. Relat. Phenom. **144–147**, 1035 (2005).
[25] C. F. Chang, Z. Hu, H. Wu, T. Burnus, N. Hollmann, M. Benomar, T. Lorenz, A. Tanaka, H. J. Lin, H. H. Hsieh, C. T. Chen, and L. H. Tjeng, Phys. Rev. Lett. **102**, 116401 (2009).
[26] Z. Hu, H. Wu, M. W. Haverkort, H. H. Hsieh, H. J. Lin, T. Lorenz, J. Baier, A. Reichl, I. Bonn, C. Felser, A. Tanaka, C. T. Chen, and L. H. Tjeng, Phys. Rev. Lett. **92**, 207402 (2004).
[27] G. van der Laan, J. Zaanen, G. A. Sawatzky, R. Karnatak, and J. M. Esteva, Phys. Rev. B **33**, 4253 (1986).
[28] G. van der Laan, C. M. B. Henderson, R. A. D. Pattrick, S. S. Dhesi, P. F. Schofield, E. Dudzik, and D. J. Vaughan, Phys. Rev. B **59**, 4314 (1999).
[29] M. Kitamura, M. Kobayashi, E. Sakai, M. Minohara, R. Yukawa, D. Shiga, K. Amemiya, Y. Nonaka, G. Shibata, A. Fujimori, H. Fujioka, K. Horiba, and H. Kumigashira, Phys. Rev. B **100**, 245132 (2019).
[30] See Supplemental Material at http://link.aps.org/supplemental/10.1103/PhysRevB.101.224434 for XAS spectra acquired from measurements at beamlines in SPring-8 and Photon Factory, estimation of the Ni valence state, and oxygen content in NCO films.
[31] C. Piamonteze, M. Gibert, J. Heidler, J. Dreiser, S. Rusponi, H. Brune, J. M. Triscone, F. Nolting, and U. Staub, Phys. Rev. B **92**, 014426 (2015).